Journal of Petroleum Science and Engineering 160 (2018) 442–451

Contents lists available at ScienceDirect

Journal of Petroleum Science and Engineering

journal homepage: www.elsevier.com/locate/petrol

Phase behavior of N_2/n-C_4H_{10} in a partially confined space derived from shale sample

Yueliang Liu [a], Huazhou Andy Li [a,*], Ryosuke Okuno [b]

[a] School of Mining and Petroleum Engineering, Faculty of Engineering, University of Alberta, Edmonton, T6G1H9, Canada
[b] Petroleum & Geosystems Engineering, University of Texas at Austin, Austin, TX 78712, USA

ARTICLE INFO

Keywords:
Partially confined space
Sorption
Bubble-point pressure
Shale sample

ABSTRACT

Phase behavior of shale fluids in small pores is not well understood. One complexity comes from the fact that sorption of components by organic-rich shale can be significant and selective. In an attempt to elucidate the effect of sorption on phase behavior of shale fluids, we present a new experimental method that can be used to measure the bubble-point pressures of N_2/n-C_4H_{10} mixtures in the presence of an actual shale sample. Pressure/volume (P/V) isotherms for a given mixture were firstly measured in a PVT cell. Then, the measurements of the P/V isotherms for the same mixture were repeated in a partially confined space by opening a valve between the PVT cell and a shale container. The so-called partially confined space consists of the pore space inside the shale sample, the bulk space in the PVT cell and in the connecting tubing, and the non-cementing pore spaces among the shale particles. Results show that, the measured bubble-point pressure of the N_2/n-C_4H_{10} mixture in the partially confined space was higher than the corresponding bubble-point pressure in the bulk space. A detailed analysis indicates that, when loaded in the partially confined space, n-C_4H_{10} exhibits a higher level of sorption capacity on the shale sample than N_2, resulting in a higher concentration of N_2 left in the free fluid than that in the initial mixture, which is the so-called selective sorption. The higher concentration of N_2 led to the higher bubble-point pressure as observed in the measurements. The increase of the bubble-point pressure due to the selective sorption was observed to be greater at a lower temperature. This is because the sorption of n-C_4H_{10} relative to that of N_2 is more significant at a lower temperature. A higher temperature did not lead to a higher increment in the bubble-point pressure likely because bubble-point is more sensitive to composition than to temperature for these mixtures at the conditions tested. This emphasizes the importance of considering sorption in phase behavior for small pores.

1. Introduction

Unlike conventional reservoirs, shale reservoir possesses unique characteristics, such as ultra-low permeability and strong heterogeneity. Nano-scale pores are dominant pores in shale reservoirs, and their diameters are normally between 1 and 20 nm (Nagarajan et al., 2013). Thermodynamics and phase equilibria of fluids in nano-pores (called "confined spaces") are more complicated than those in bulk spaces. In such pores, the in-situ phase behavior in confined spaces is affected by pore wall-fluid interaction, capillary pressure, and sorption of hydrocarbon on shale material (Li et al., 2014; Jin and Firoozabadi, 2016).

Extensive studies are devoted to understanding the phase behavior of shale fluids. Some modeling studies were conducted to describe phase behavior of shale fluids in confined spaces. Nojabaei et al. (2013) coupled capillary pressure with phase equilibrium relation to describe phase behavior of confined fluids by use of the Peng-Robinson equation (PR EOS) (Peng and Robinson, 1976). They reported that small pores decreased bubble-point pressures, and either decreased or increased dew-point pressures. Travalloni et al. (2014) modeled phase behavior of confined fluids in homogeneous and heterogeneous porous media using an extended PR EOS. Their modeling study showed that small pores may confine phases with very similar or very different densities and compositions. Dong et al. (2016) numerically studied phase equilibrium of pure components and their mixtures in cylindrical nano-pores using the PR EOS coupled with capillary pressure and adsorption theory. The reduction of pore diameter was considered in their model due to the existence of adsorption film. Wang et al. (2016) numerically investigated the effect of pore size distribution on phase transition of hydrocarbon mixtures in

* Corresponding author. Petroleum Engineering, University of Alberta, Canada.
E-mail address: huazhou@ualberta.ca (H.A. Li).

https://doi.org/10.1016/j.petrol.2017.10.061
Received 14 June 2017; Received in revised form 27 September 2017; Accepted 21 October 2017
Available online 23 October 2017

nano-porous media. They presented a procedure to simulate the sequence of phase transition in nano-porous media, and found that a phase change always occurs firstly in the larger pores, and then in the smaller pores.

Experimental studies on the phase behavior of fluids contained in the nano-pore spaces of shale are, however, relatively scarce in the literature. Morishige et al. (1997) measured adsorption isotherms of pure gases on meso-porous MCM-41 molecular sieves with different pore sizes. Their experimental adsorption data showed that the critical temperatures of pure fluids in meso-pores were quite different from those in the bulk space. Yan et al. (2013) applied differential scanning calorimetry and temperature-dependent X-ray diffraction technology to obtain phase behavior of n-tridecane/n-tetradecane mixtures in the bulk and in the confined porous glass. The mixtures showed a similar phase behavior to the bulk, especially in larger pores than 30 nm. Under confinement, their phase behavior varied with pore size as well as temperature and composition. Wang et al. (2014) applied nano-fluidic devices to visualize phase changes of pure alkane and alkane mixtures under nano-confinement. The vaporization of liquid phase in nano-channels (5 μm wide by 100 nm deep) was remarkably suppressed in comparison to that in micro-channels (10 μm wide by 10 μm deep). Pure alkanes and alkane mixtures exhibited different vaporization behavior; this was because the liberation of lighter components from the liquid phase to the gas phase in the micro-channels increased the apparent molecular weight of the liquid in the nano-channels, suppressing its bubble point (Wang et al., 2014). Alfi et al. (2016) investigated phase behavior of pure Hexane, Heptane, and Octane inside nano-channels of 50 nm using lab-on-a-chip technology integrated with high-resolution imaging techniques. They found that, in a nano-channel with a width of 50 nm, the confinement effect in the form of wall-molecule interactions was almost negligible. Luo et al. (2016) experimentally explored the relationship between saturation temperature and pore diameter for n-hexane, n-octane, and n-decane that were confined in silicate nano-porous materials CPG-35 using differential scanning calorimetry. They observed that the saturation temperature in nano-pores was higher than that in a bulk space.

To summarize, extensive studies have been conducted to elucidate the effect of capillary pressure on the phase behavior of confined fluids. However, the effect of sorption on the phase equilibrium of shale fluids is scarcely investigated, although it is an important and common phenomenon in shale reservoirs. To our knowledge, no publications have reported experimental data on the phase behavior of fluids in the presence of real shale materials.

n-C_4H_{10}, as a nonvolatile hydrocarbon, is a common component present in the shale gas-condensate reservoirs; N_2, as a volatile non-hydrocarbon component, can be introduced into the reservoir as an energized fluid used during an energized fracturing treatment. Furthermore, N_2 has been found to be an essential component that can be produced from some shale reservoirs, e.g., Antrim shale and Barnett shale. Hence, the N_2/n-C_4H_{10} binary is selected to elaborate the effect of sorption on the in-situ phase behavior of shale fluid. This paper presents an experimental study on the phase behavior of two binary mixtures in a partially confined space. Fig. 1 illustrates the physical model representing a partially confined space, which consists of a bulk space and a confined space. The major objective is to explore the impact of sorption on fluid phase behavior. The experimental section shows the materials, the experimental setup and the procedures adopted in this study. Bubble-point pressures for the binary mixtures were measured firstly in a bulk space, and then in a partially confined space. The results and discussion section presents the experimental results and major findings in this study. We delineate the reasons leading to differences in bubble-point pressure between the bulk and the partially confined space. To our knowledge, this is the first time that the effect of sorption on the phase behavior of fluid mixtures in the presence of real shale is measured.

2. Experimental section

2.1. Materials

The purities of N_2 and n-C_4H_{10} (Praxair, Canada) used in this research are 99.998 mol% and 99.99 wt%, respectively. Two hydrocarbon-wetting shale cores were used in the tests. Both shale cores (#1 and #2) were retrieved from Devonian formation in Canada.

2.2. Experimental setup

Pressure/volume (P/V) isotherm measurements for N_2/n-C_4H_{10} mixtures were carried out with a conventional PVT apparatus (Schlumberger DBR, Edmonton, Canada). The operation limits for the PVT cell equipped in the PVT setup are 200,000 kPa and 473.15 K. The total sample capacity of the PVT cell is 124.0 cm^3. The pressure of the PVT cell is controlled by a high-pressure positive displacement pump (PMP-500-1-20-HB, Schlumberger DBR, Edmonton, Canada). The temperature of the system is controlled by an air bath with an accuracy of ±0.1 K. A cathetometer directly measures a fluid volume in the PVT cell by the

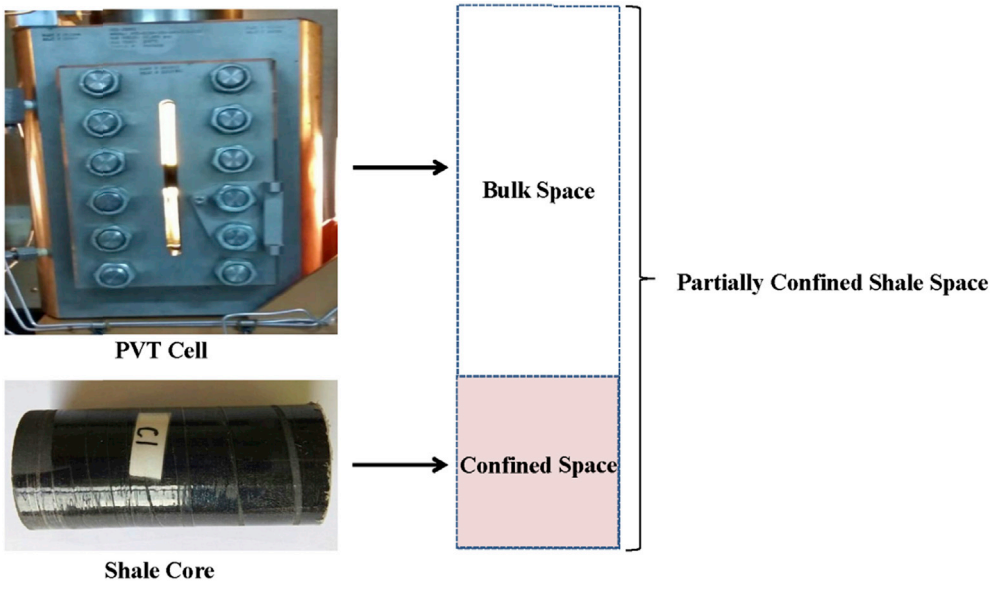

Fig. 1. Schematic diagram of the partially confined space that consists of a bulk space and a confined shale space.

height of the fluid. The uncertainty of the volume measurement is ±0.016 cm^3. In order to obtain a highly accurate fluid pressure, a pressure gauge (901A-15K-232P-R5, Ashcroft Inc, Stratford, USA) was used to measure the fluid pressure with an accuracy of ±1 kPa.

2.3. Experimental procedures

This section describes the N_2 adsorption/desorption test used for characterizing both shale cores (#1 and #2), the procedure of total organic carbon (TOC) measurement for shale cores, the measurement of system volumes, and the constant composition expansion (CCE) method for measuring P/V isotherms. Fig. 2 shows the schematic diagram of the experimental setup for measuring P/V isotherms of N_2/n-C_4H_{10} mixtures.

Before the measurement, both shale cores (#1 and #2) were placed in an oven, and vacuumed for 48 h and heated at a constant temperature of 423.15 K with helium as a carrier gas to remove moisture and other adsorbed gases. This pretreatment was called "degassing and drying treatment". Helium within the shale samples was then evacuated prior to any further treatments. After this treatment, the surface area was artificially increased by crushing the shale cores into small particles with diameters in the range of 1.00–1.18 mm (US Mesh 16–18). The shale particles were then collected and stored in a zip-locked bag to avoid oxidation and water uptake.

Pore size distribution of the shale particles was then characterized by N_2 adsorption/desorption test. The N_2 adsorption/desorption test on shale samples #1 and #2 was conducted with the Autosorb iQ-Chemisorption & Physi-sorption Gas Sorption Analyzer (Quantachrome Instruments, USA). The range of pore width that can be detected by this apparatus is 0.35–500 nm. It took about 3–4 h for N_2 to reach adsorption/desorption equilibrium with the shale samples at a given temperature and pressure.

Furthermore, the pore volume of both shale samples was obtained with the Quantachrome Autosorb software installed for the gas sorption analyzer. Based on the assumption that the pores present in the solid particles are cylindrical, the software can figure out the total pore volume in the particles by measuring the total amount of N_2 take-up at 101.325 kPa and 77 K. From N_2 adsorption/desorption test, the pore volume, and pore size distribution for each shale core were obtained with an accuracy of ±0.6%.

Part of the shale particles were then used for the TOC test. The TOC of both shale cores was measured by a combustion elemental analyzer. During the measurement, H_2SO_4 (10 wt%) was added to the shale particles; then the solution was sparged with oxygen until the purgeable organic carbon and inorganic carbon were removed. The non-purgeable organic carbon was then placed in the combustion tube to form carbon dioxide, which can be detected by the non-dispersive infrared detector. Then, the TOC was obtained. Table 1 lists the mass, pore volume, and TOC of the two shale samples.

The system volume was measured after shale core characterization. In order to obtain an accurate P/V isotherm for fluid mixtures in the partially confined space, it is crucial to obtain an accurate total volume of the mixture. The total volume of the mixture in the partially confined space is calculated as

$$V_{Total} = V_{Cell} + V_{Cell}^{Dead} + V_{Tubing} + V_{Container} + V_{Pore} - V_{Particle} \quad (1)$$

where V_{Total} is the total volume of the mixture in the partially confined space, cm^3; V_{Cell} is the volume of the mixture in the PVT cell, cm^3; V_{Cell}^{Dead} is the dead volume of the PVT cell; V_{Tubing} is the inner volume of stainless steel-tubing lying between the PVT cell and the shale container, cm^3; $V_{Container}$ is the total volume of the shale container, cm^3; V_{Pore} is the total pore volume in the shale particles, cm^3; and $V_{Particle}$ is the total volume of shale particles including both the pore volume and the solid volume, cm^3.

During the experiment, V_{Cell} was obtained by using a cathetometer through measuring the height of the fluid system with an accuracy of ±0.016 cm^3. V_{Cell}^{Dead} is 1.754 cm^3. By employing Boyle-Charles' law, V_{Tubing} was measured as 3.517 cm^3 with an accuracy of ±0.010 cm^3. $V_{Container}$ in this experiment is 10.000 cm^3. V_{Pore} was measured by N_2 adsorption/desorption test. After each P/V isotherm measurement, $V_{Particle}$ was measured through a drainage method by immersing the shale particles into distilled water contained in a cylinder; the volume change before and after the immersion gave the total volume of the shale particles. Considering that the shale material was hydrocarbon-wetting, it is reasonable to assume the distilled water could not enter nano-pores in the shale particles. Thus, $V_{Particle}$ is approximately equal to the volume change of water in the cylinder.

Table 2 shows the compositions of two N_2/n-C_4H_{10} mixtures, molar numbers of each component injected and testing temperatures. Before each P/V isotherm measurement, the entire PVT system was tested for leakage with N_2 with testing pressure set as high as 20,000 kPa. Then, it

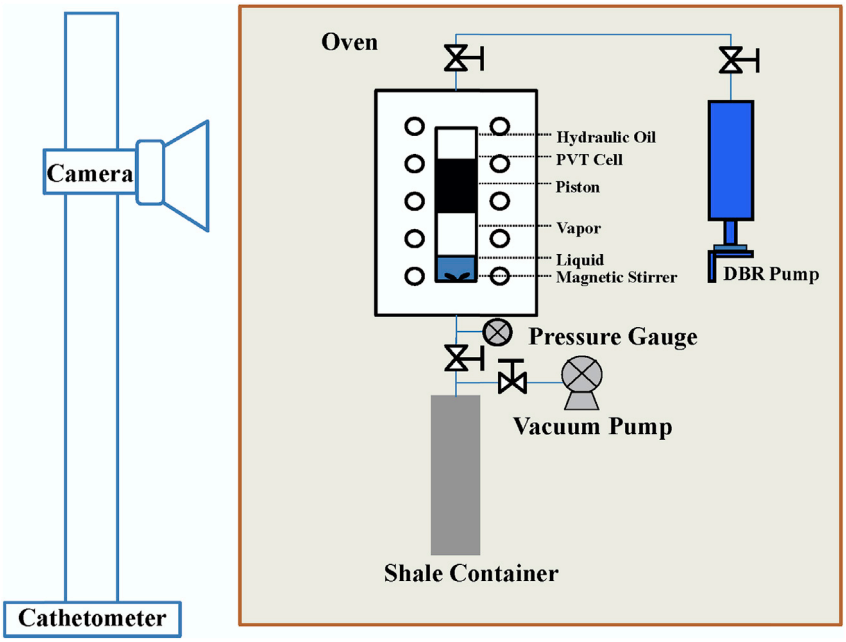

Fig. 2. Schematic diagram of the experimental setup for measuring equilibrium P/V isotherms.

Table 1
Properties of the two shale samples used in this study.

Shale Sample	Mass, g	Pore Volume, cm^3/g	TOC, w/w%	Clay Composition, wt %		Other Minerals, wt%			
				Illite	Smectite	Quartz	Potassium feldspar	Plagioclase	Calcite
#1	19.015	0.0211	0.988	31.0	32.0	26.0	1.6	3.0	6.4
#2	18.230	0.014	2.217	25.0	34.0	18.0	3.2	9.7	10.1

Table 2
Compositions and molar numbers of the N_2/n-C_4H_{10} mixtures tested in this study. For each mixture, experiments were conducted at two temperatures: 299.15 K and 324. 15 K.

Molar Percentage		Molar Numbers	
N_2, mol%	n-C_4H_{10}, mol%	N_2, mol	n-C_4H_{10}, mol
5.40	94.60	0.0140	0.2452
5.01	94.99	0.0131	0.2476

was cleaned with acetone, and evacuated using a vacuum pump for 2 h. Shale particles were then placed in the shale container and connected with the PVT cell. The whole system was evacuated again for 12 h using a vacuum pump. In order to prevent shale particles from flowing away during evacuating, a steel mesh with mesh number 200 was used at the outlet of the shale container.

A high-pressure cylinder containing a sufficient amount of n-C_4H_{10} was connected to the PVT cell, allowing direct withdrawal of the liquid n-C_4H_{10} into the PVT cell. A certain amount of liquid n-C_4H_{10} was injected into the PVT cell just above its vapor pressure at room temperature. Then the air bath temperature was set to be 303.15 K for 12 h, enabling the n-C_4H_{10} sample in the PVT cell to reach thermal equilibrium. Then, the moles of the injected n-C_4H_{10} can be obtained according to its density and its volume measured by the accurate cathetometer. Its density is obtained from the National Institute of Standards and Technology (NIST) (Linstrom and Mallard, 2017). Then, N_2 was added into the PVT cell without turning on the magnetic stirrer. After injection, the mixture was then pressurized into single-liquid state with the magnetic stirrer being turned on for 6 h. The mixture was maintained at 303.15 K for 12 h, enabling it to reach a thermal equilibrium. Bubble-point pressures for this mixture in the PVT cell were measured by the constant composition expansion (CCE) method. Because the vapor-liquid equilibrium of N_2/n-C_4H_{10} mixtures is predicted quite well with the PR EOS model (Robinson and Peng, 1978; Myers and Sandler, 2002), the composition of the binary mixture is determined by a PR EOS model fitted to match the measured bubble-point pressure. The physical properties of pure components and their binary interaction parameters used with the PR EOS are shown in Table 3. This method for determining the binary-mixture composition has an accuracy of ±0.3% on the basis of the cross-checking with the composition measured by gas chromatography (GC) tests. After the determination of the overall composition, the system temperature was set to an operating temperature. Subsequently, we vigorously stirred the mixture for 6 h by the magnetic stirrer at the selected operating temperature.

P/V isotherms of N_2/n-C_4H_{10} mixtures were firstly measured in the PVT cell. Subsequently, another set of P/V isotherms for the same mixture were measured in the partially confined space by connecting the PVT cell with the shale container. Crushed shale particles with a certain mass were loaded in the shale container. The container and the tubing between the PVT cell and container were sufficiently vacuumed prior to being connected to the PVT cell. At each temperature, P/V isotherm measurement was initiated from a single-liquid phase state. Then, the pressure was gradually decreased to measure a P/V isotherm for the mixture. The mixture was sufficiently stirred for 30 min to ensure an equilibrium state prior to each volume measurement. After stirring, the magnetic stirrer was switched off and sufficient time, about 4–6 h, was allowed to reach an equilibrium state. The equilibrium was indicated when no pressure changes were observed for a period of 2 h. Thereafter, phase equilibrium of the mixture was visually identified, and the pressure and volume of each phase were measured and recorded. A phase boundary was confirmed by plotting the total volume with respect to pressure and locating the transition point in the curve. The P/V relationship often shows a clear slope change when the vapor phase appears as pressure reduces. The uncertainty in the measurement of the bubble-point pressure as well as the equilibrium pressures is estimated to be ±2.5%. To make sure the measured P/V isotherms are reliable and reproducible, we conducted two runs of constant composition expansion experiments to measure the P/V isotherms of the N_2/n-C_4H_{10} mixture (5.40 mol%, 94.60 mol%) in the PVT cell with (or without) shale sample #1 at 299.15 K. The maximum deviation between the results obtained with the two consecutive runs is found to be less than ±3.8%.

Table 3
Physical properties of pure components and their binary interaction parameters used in the PR EOS (1978) model.

Components	Critical Temperature, K	Critical Pressure, kPa	Acentric Factor	Binary Interaction Parameter	
				n-C_4H_{10}	N_2
n-C_4H_{10}	425.2	3799.6875	0.193	0.000	0.095
N_2	126.2	3394.3875	0.040	0.095	0.000

3. Results and discussion

3.1. Characterization of shale samples

Figs. 3–4 show the measured pore size distributions of the shale samples #1 and #2, respectively, as obtained through N_2 adsorption/desorption test. Fig. 3 indicates that shale sample #1 contains pores falling in the range of 1–20 nm. The single sharp peak indicates that shale sample #1 has a narrow pore size distribution around 5.0 nm. In contrast, Fig. 4 shows that shale sample #2 has a wider pore size distribution in the range of 1–70 nm.

It can be seen from Table 1 that the TOC content in shale sample #2 is 2.24 times higher than that in the shale sample #1. Previous studies showed that shale materials with a higher TOC content exhibited a higher sorption capacity (Lu et al., 1995; Jarvie, 2004; Zhang et al., 2012; Clarkson and Haghshenas, 2013). Hence, shale sample #2 is expected to possess a higher sorption capacity than the shale sample #1. In Section 3.3, we will present the sorbed molar numbers of N_2 and n-C_4H_{10} on the two shale samples, and in Section 3.4, we will explore the possible relationships between TOC content and sorption capacity of individual components.

3.2. Phase behavior of N_2/n-C_4H_{10} mixtures in the partially confined space

The P/V isotherms for the N_2/n-C_4H_{10} mixtures, together with the measurement uncertainties, are shown in Figs. 5–8. In Figs. 5–8, the solid squares represent the P/V isotherms measured in the PVT cell, and the solid circles represent the P/V isotherms measured in the partially confined space. As depicted in Figs. 5–8, the phase boundary between single-phase region and two-phase region can be estimated by the

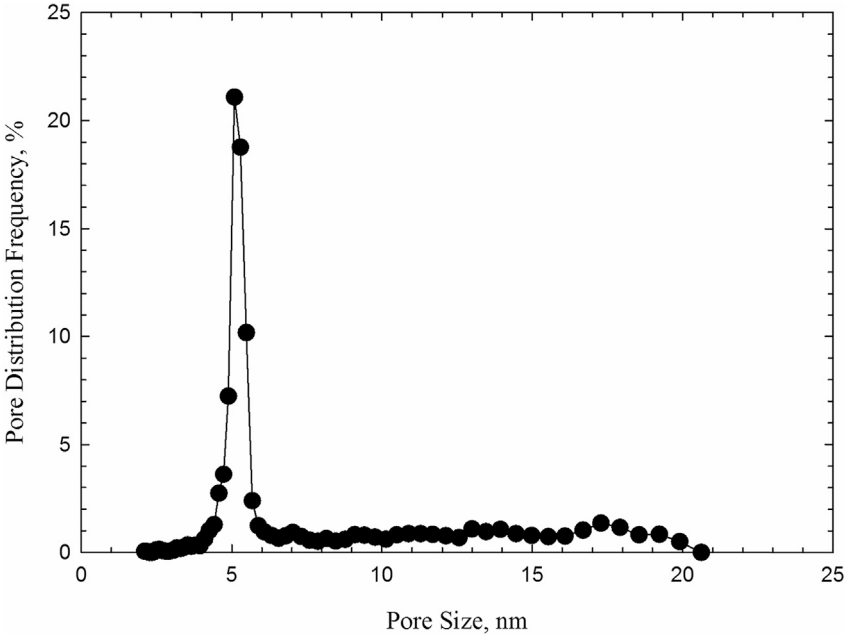

Fig. 3. Pore size distribution of shale sample #1 as measured by the N_2 adsorption/desorption test.

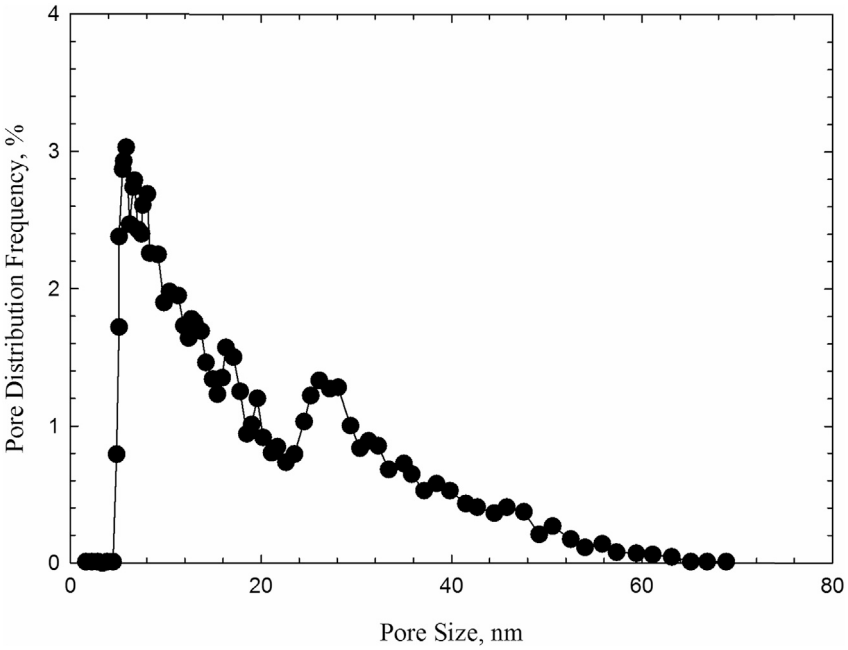

Fig. 4. Pore size distribution of shale sample #2 as measured by the N_2 adsorption/desorption test.

intersection of two trend lines drawn to represent the two types of phase equilibrium. The dashed line in Figs. 5–8 represents the bubble-point pressures of the N_2/n-C_4H_{10} mixtures that are calculated with the PR EOS (1978).

Figs. 5–8 show that a good agreement is observed between the measured and calculated bubble-point pressures. We can observe the bubble-point pressures of the N_2/n-C_4H_{10} mixtures in the partially confined space are higher than those measured in the bulk space. Table 4 shows the detailed changes in the bubble-point pressure of the mixtures after being sorbed on the two shale samples. Previous studies reported that when a multi-component mixture contacts with a shale sample, different components in the mixture exhibit different levels of sorption on shale, leading to the so-called selective sorption phenomenon (Haghshenas et al., 2014; Wang et al., 2015). In this study, the shale particles were always immersed into the single-liquid phase during the measurements. The liquid N_2 and n-C_4H_{10} were deemed to sorb on shale samples with different sorption levels at a given temperature and pressure. The selective sorption of N_2 and n-C_4H_{10} changes the initial composition of the N_2/n-C_4H_{10} mixtures, and thus results in an increase in bubble-point pressure, as demonstrated in Figs. 5–8.

Previous studies demonstrated that bubble-point pressure can be reduced due to the capillary pressure present in small pores (Devegowda et al., 2012; Nojabaei et al., 2013; Teklu et al., 2014). Capillary pressure is attributed to the interfacial tension that exists across the curved interface between the vapor/liquid phases in a tube (Firoozabadi, 2016). Wang et al. (2014, 2016) studied phase behavior of a fluid contained in a

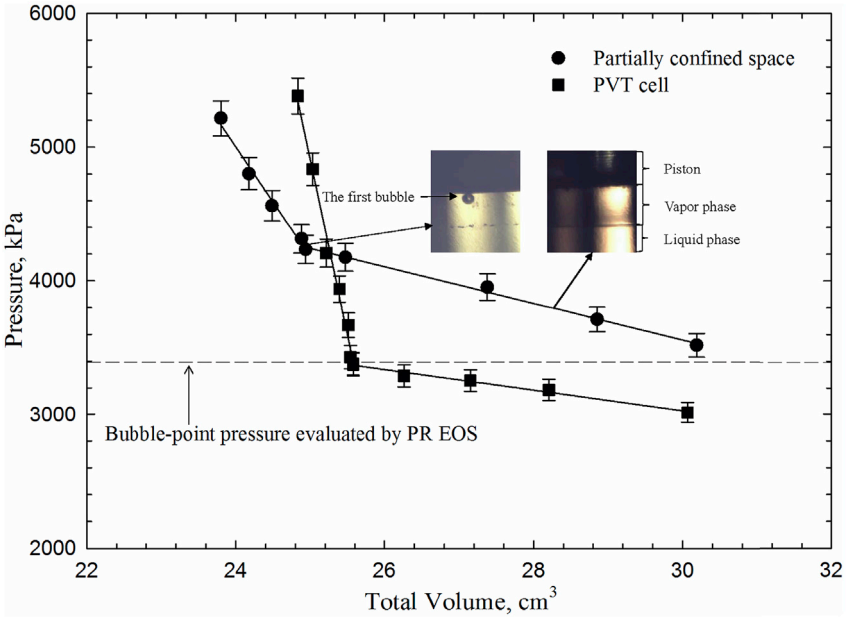

Fig. 5. Measured P/V isotherms for the N_2/n-C_4H_{10} mixture with composition of (5.40 mol%, 94.60 mol%) in the PVT cell with and without shale sample #1 at 299.15 K.

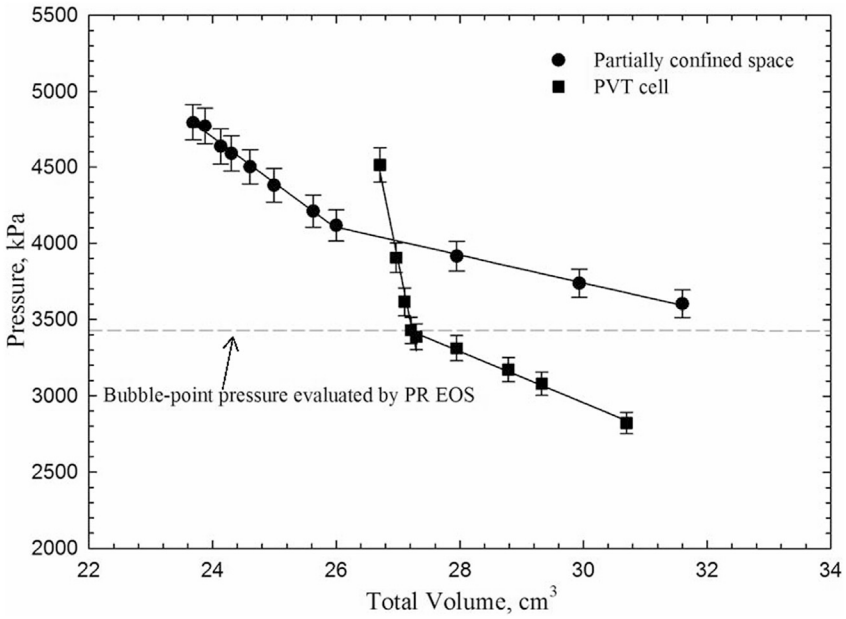

Fig. 6. Measured P/V isotherms for the N_2/n-C_4H_{10} mixture with composition of (5.40 mol%, 94.60 mol%) in the PVT cell with and without shale sample #1 at 324.15 K.

porous medium with a pore size distribution; they presented that if the fluid was initially a single-liquid phase during the constant composition expansion (CCE) process, the vapor phase would firstly appear in larger pores, and then appear in smaller pores when all the liquid vaporized in the larger pores. In this study, if we regard the PVT cell as a pore with an infinite pore radius, the first bubble is expected to arise from the PVT cell during the CCE test based on Wang et al. (2014, 2016). During the measurements, the shale samples were always immersed into the single-liquid phase. At the bubble-point, therefore, the fluid contained in the shale pores was always a single-liquid phase and no capillary pressure was present in the shale pores. We deduced that the measured bubble-point pressure in the partially confined space should be influenced only by the effect of selective sorption between individual components (N_2 and n-C_4H_{10} in this study), without the effect of capillary pressure.

3.3. Sorption of individual components on shale samples

This section quantifies the selective sorption between the two components by calculating sorbed molar numbers on the two shale samples based on the results given in Table 4. It is explained how selective sorption is expected to affect the bubble-point pressure of a mixture in a partially confined space.

Shale gas-condensate reservoirs, which are normally organic-rich, are traditionally referred as “sorbed gas” reservoirs because a significant amount of shale gas is stored through physical adsorption onto the internal rock surface and through absorption within organic matter (Clarkson and Haghshenas, 2013). Based on the previous research findings, in this research, it can be reasonably deduced that N_2 and n-C_4H_{10} not only adsorb onto the shale rock surface, but also absorb within the organic matter at given temperature and pressure. In addition, Clarkson

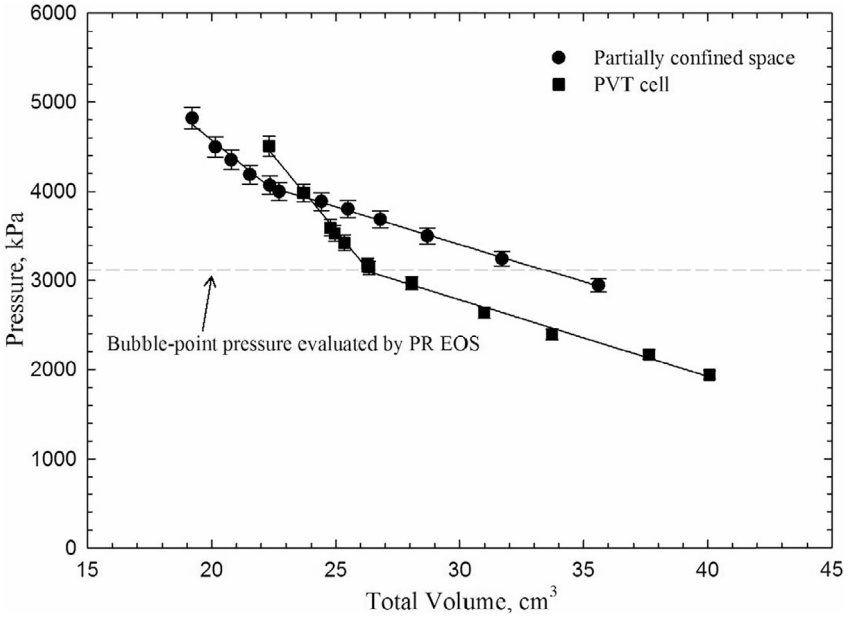

Fig. 7. Measured P/V isotherms for the N_2/n-C_4H_{10} mixture with composition of (5.01 mol%, 94.99 mol%) in the PVT cell with and without shale sample #2 at 299.15 K.

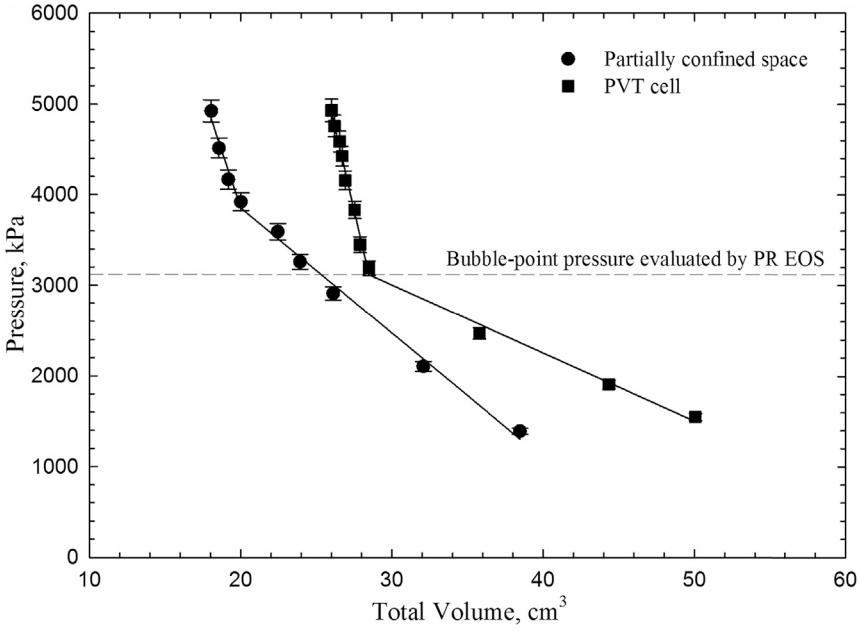

Fig. 8. Measured P/V isotherms for the N_2/n-C_4H_{10} mixture with composition of (5.01 mol%, 94.99 mol%) in the PVT cell with and without shale sample #2 at 324.15 K.

Table 4
Changes in the bubble-point pressure of N_2/n-C_4H_{10} mixtures when they are equilibrating with the two shale samples. Note that the experimental temperatures are above the supercritical temperature of N_2. The bubble-point pressure of n-C_4H_{10} at 299.15 K and 324.15 K are 241.0 kPa and 523.0 kPa, respectively.

Shale Sample	Molar Percentage		Temperature, K	Bubble-Point Pressure in the PVT cell, kPa	Bubble-Point Pressure in the Partially Confined Space, kPa	Percentage Change in Bubble-Point Pressure, %
	N_2, mol%	n-C_4H_{10}, mol%				
#1	5.40	94.60	299.15	3390.6	4268.5	25.89
	5.40	94.60	324.15	3429.5	4105.8	19.72
#2	5.01	94.99	299.15	3115.1	4035.5	29.55
	5.01	94.99	324.15	3189.6	3883.8	21.76

and Haghshenas (2013) proposed five mechanisms for gas storage in shale gas-condensate reservoirs: (1) Adsorption on internal surface area; (2) Compressed gas storage in natural and hydraulic fractures; (3) Compressed gas storage in matrix porosity; (4) Dissolved gas in formation water; and (5) Absorption in organic matter. Similarly, in our study, N_2 and n-C_4H_{10} in the partially confined space can exhibit two storage states; one is the sorbed gas including adsorption on shale rock surface and absorption in organic matter, and the other is the unsorbed gas which

includes the compressed gas located in the pore space inside the shale sample, the bulk space in the PVT cell and in the connecting tubing, and the non-cementing pore spaces among the shale particles.

During the P/V isotherm measurements, as the fluid mixture in the partially confined space was depressurized, the first bubble liberated from the single-liquid phase (See Fig. 5). At such a bubble-point, the composition of the N_2/n-C_4H_{10} mixture in the partially confined space was different from that of the initial mixture loaded in the bulk space. This difference was caused by the selective sorption between N_2 and n-C_4H_{10} on shale samples. In order to obtain the sorbed molar numbers of N_2 and n-C_4H_{10} on the shale samples, we firstly calculated the unsorbed moles of the mixture based on the following three assumptions: (1) The volume of the sorbed layers was negligible in comparison with V_{Total}; (2) The distribution of the unsorbed gas was homogeneous in all spaces; and (3) The interactions of unsorbed/sorbed molecules and unsorbed molecules/pore wall were neglected. Then, the following equation was employed to compute the total molar numbers of the unsorbed N_2/n-C_4H_{10} mixture in the partially confined space,

$$n_p = \frac{P_b V_{Total}}{Z_p RT} \tag{2}$$

where n_p is the total molar number of the unsorbed N_2/n-C_4H_{10} mixture in the partially confined space, mol; P_b represents the bubble-point pressure of the unsorbed N_2/n-C_4H_{10} mixture in the partially confined space, Pa; V_{Total} represents the total volume of the unsorbed N_2/n-C_4H_{10} mixture in the partially confined space, m^3, Z_p is the compressibility factor of the unsorbed N_2/n-C_4H_{10} mixture in the partially confined space that is calculated by the PR EOS; R is the universal gas constant, 8.314 m^3 Pa·K^{-1}·mol^{-1}; and T is the temperature, K.

After obtaining the total molar numbers of the unsorbed N_2/n-C_4H_{10} mixture in the partially confined space, the sorbed molar numbers of N_2 and n-C_4H_{10} can then be determined at the bubble point with the following equations, respectively,

$$n_{ad\_N_2} = n_o x_{N_2} - n_p x'_{N_2} \tag{3}$$

$$n_{ad\_C_4} = n_o x_{C_4} - n_p x'_{C_4} \tag{4}$$

where n_{ad_N2} and n_{ad_C4} are the sorbed molar numbers of N_2 and n-C_4H_{10} on shale samples, respectively, mol; n_o is the injected molar number of the N_2/n-C_4H_{10} mixture, mol; x_{N2} and x_{C4} are the molar percentage of N_2 and n-C_4H_{10} in the injected mixture in the PVT cell, respectively; x'_{N2} and x'_{C4} are the molar percentage of N_2 and n-C_4H_{10} when the mixture rests at the bubble-point in the partially confined space, respectively. Equations (3) and (4) are derived based on the assumption that the distribution of the unsorbed gas is uniform in all spaces as mentioned above.

Table 5 lists the calculated molar percentages of N_2 and n-C_4H_{10} in the mixture before and after sorption, and sorbed molar numbers of N_2 and n-C_4H_{10} in the partially confined spaces. The higher sorption tendency of n-C_4H_{10} than that of N_2 is indicated in calculated sorbed molar numbers in Table 5. The molar percentage of N_2 in mixture in the partially confined space tends to increase in comparison to that in the bulk space. The higher N_2 concentration results in the higher bubble-point pressure of the N_2/n-C_4H_{10} mixture in the partially confined space, as observed in Figs. 5–8.

Table 5 also shows that, for a given N_2/n-C_4H_{10} mixture, both N_2 and n-C_4H_{10} sorb more at a lower temperature. A higher temperature did not lead to a higher bubble-point pressure for a given mixture (Table 4) likely because bubble-point is more sensitive to composition than to temperature for these mixtures at the conditions tested. This emphasizes the importance of considering sorption in phase behavior calculation for small pores.

3.4. Effect of TOC on sorption capacity

In this study, sorption capacity is defined as the ability of gas storage on shale; quantitatively, it is equal to the sorbed molar numbers per gram of shale rocks. Organic matters present in shale rocks, generally represented by TOC content, can sorb and store shale components. Previous studies have investigated the relationship between TOC content and sorption capacity, showing that an increase in TOC content can lead to an approximately linear increase in the sorption capacity (Lu et al., 1995; Jarvie, 2004; Zhang et al., 2012). In this study, Table 5 also shows, given the fact that the two N_2/n-C_4H_{10} mixtures have a similar composition, much more N_2 and n-C_4H_{10} are sorbed onto the shale sample #2 than the shale sample #1 under similar temperature/pressure conditions. This can be attributed to a higher TOC content in the shale sample #2 than the shale sample #1.

Sorption capacities of N_2 and n-C_4H_{10} are closely correlated with the TOC content in the shale samples. Charoensuppanimit et al. (2016) measured N_2 and CH_4 sorption on shale materials and found both of their sorption capacities are positively correlated with TOC content. As for the sorption of n-C_4H_{10} on shale materials, however, there is no data available in the literature. Considering that CH_4 and n-C_4H_{10} are both hydrocarbons and have natural affinity with TOC content, it is conceivable that the sorption capacity for n-C_4H_{10} is correlated with TOC content positively.

After obtaining the sorbed molar numbers of individual components in each shale sample, the sorption capacities of N_2 and n-C_4H_{10} on two shale samples can be calculated by the following equation,

$$V_{ad} = \frac{n_{ad}}{m} \tag{5}$$

where V_{ad} represents the sorption capacity, mmol/g; n_{ad} is the sorbed molar numbers of individual components in each shale sample, mmol; m is the mass of the shale sample, g.

Figs. 9 and 10, respectively, show the sorption capacities of N_2 and n-C_4H_{10} in terms of the TOC content in both shale samples. The sorption capacity for n-C_4H_{10} increases with the increasing TOC content, while the sorption capacity for N_2 only increases slightly with the TOC content. A shale sample with a higher TOC content is expected to have a higher sorption capacity, which is consistent with the findings by Nuttall et al. (2005) that sorption occurs primarily on active sites containing organic carbons. Besides, the natural affinity between hydrocarbon n-C_4H_{10} and TOC content leads to a higher sorption of n-C_4H_{10} as compared to non-hydrocarbon N_2. However, it seems that the sorption amount is not affected much by the TOC content of shale sample #1 and #2. Recently, Xiong et al. (2017) conducted a series of methane sorption measurements for seven shale core samples collected from the Ordos Basin with depths

Table 5
Calculated molar percentages of N_2 and n-C_4H_{10} in the mixture before and after sorption, and sorbed molar numbers of N_2 and n-C_4H_{10} at the bubble-point in the partially confined spaces. Note that the molar concentrations of N_2 and n-C_4H_{10} have been determined by the PR EOS (1978) calibrated with the measured bubble-point.

Shale Sample	Temperature, K	Molar Percentage before Sorption		Molar Percentage after Sorption		Adsorbed Molar Numbers	
		N_2, mol%	n-C_4H_{10}, mol%	N_2, mol%	n-C_4H_{10}, mol%	N_2, mol	n-C_4H_{10}, mol
#1	299.15	5.40	94.60	7.00	93.00	0.0007	0.0683
#1	324.15	5.40	94.60	6.70	93.30	0.0006	0.0583
#2	299.15	5.01	94.99	6.59	93.41	0.0008	0.0728
#2	324.15	5.01	94.99	6.25	93.75	0.0007	0.0612

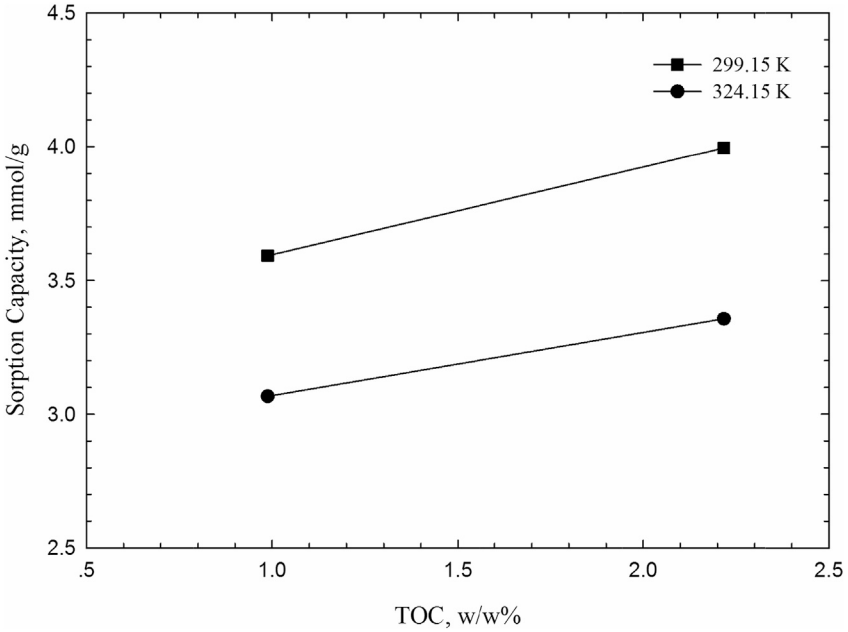

Fig. 9. Sorption capacity of n-C_4H_{10} in terms of TOC content on the two shale samples.

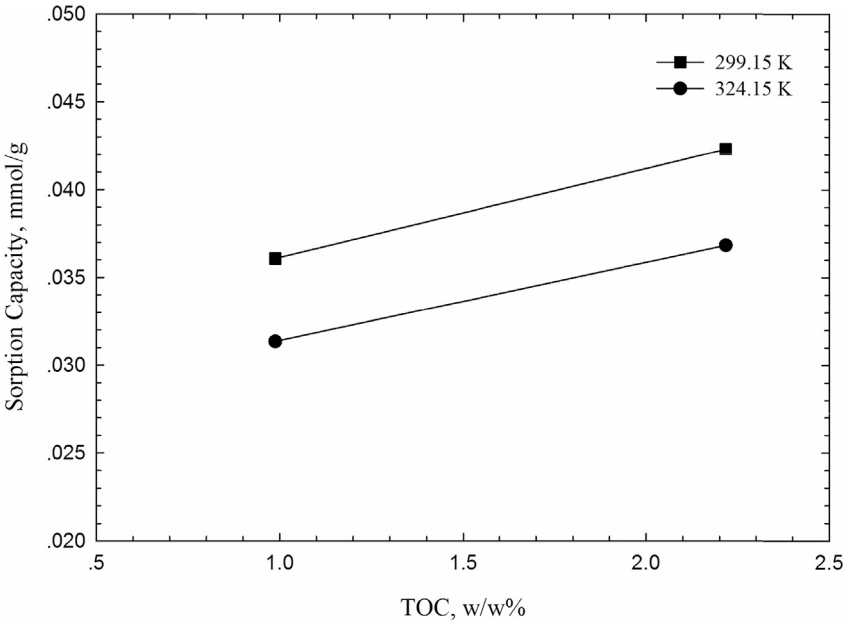

Fig. 10. Sorption capacity of N_2 in terms of TOC content on the two shale samples.

over 3000 m and TOCs ranging between 0.49 and 3.82%. They then proposed that the sorption capacity did not correlate only with the TOC content but showed a more complex dependence on petrophysical and mineralogical properties. More sorption measurements should be conducted by considering other essential factors (such as types of clay minerals) to enable more thorough understanding on the dependence of the sorption capacity of N_2 or n-C_4H_{10} on the major influential factors.

4. Conclusions

This paper presented a novel experimental method to measure phase boundaries of a fluid mixture in the presence of real shale sample retrieved from Devonian formation in Canada. In the new method, P/V isotherms were firstly measured as conventionally done with a PVT cell. Then, the P/V isotherm measurements were repeated in a partially confined space by opening a valve between the PVT cell and a shale container. In this study, P/V isotherms at two temperatures were measured for two N_2/n-C_4H_{10} mixtures in the PVT cell and in the partially confined space. Conclusions are as follows:

- It was observed that bubble-point pressures of the N_2/n-C_4H_{10} mixtures in the partially confined space were higher than those in the bulk space. A detailed analysis of results indicated that n-C_4H_{10} exhibited a higher level of sorption on the shale sample than N_2 in the partially confined space; therefore, the N_2 concentration in the free fluid was higher than that in the initial mixture. The higher N_2 concentration led to the higher bubble-point pressure as observed in the measurements.
- The increase in bubble-point pressure due to the selective sorption was observed to be greater at the lower temperature for the two

mixtures tested. This is because the sorption of n-C_4H_{10} relative to that of N_2 is more significant at the lower temperature. The observed bubble-point increases are unlikely because of capillary pressure in the shale sample, because the shale sample was placed in a liquid phase at all times during the bubble-point measurements. It was visually confirmed that the bubble-points measured were associated with appearance of the first bubble in the PVT cell.

- It was found that a larger sorption amount of N_2 and n-C_4H_{10} for a given N_2/n-C_4H_{10} mixture occurred at the lower temperature. A higher temperature did not lead to a higher bubble-point pressure for a given mixture likely because bubble-point is more sensitive to composition than to temperature for these mixtures at the conditions tested. This emphasizes the importance of considering sorption in phase behavior calculation for small pores.
- Shale sample #2 has a higher sorption capacity, especially for the hydrocarbon component n-C_4H_{10}, since its TOC content is much higher than the shale sample #1.

Acknowledgments

The authors greatly acknowledge a Discovery Grant from the Natural Sciences and Engineering Research Council of Canada of Canada to H. Li [NSERC RGPIN 05394] and China Scholarship Council for financial support to Y. Liu [201406450028]. R. Okuno holds the Pioneer Corporation Faculty Fellowship in Petroleum Engineering at the University of Texas at Austin. The first author also thanks Mr. Todd Kinnee for his experimental support. This paper is a substantially modified and improved version of SPE 181716, which was presented at the SPE Annual Technical Conference and Exhibition, 26–28 September, Dubai, UAE. The authors also thank the Alberta Geological Survey for providing the shale samples.

References

Alfi, M., Nasrabadi, H., Danerjee, D., 2016. Experimental investigation of confinement effect on phase behavior of hexane, heptane and octane using lab-on-a-chip technology. Fluid Phase Equilibr 423, 25–33.

Charoensuppanimit, P., Mohammad, S.A., Gasem, K.A.M., 2016. Measurements and modeling of gas adsorption on shales. Energy fuels. 30, 2309–2319.

Clarkson, C.R., Haghshenas, B., 2013. Modeling of supercritical fluid adsorption on organic-rich shales and coal. In: SPE Unconv. Resour. Conf. Woodlands, Texas, USA.

Devegowda, D., Sapmanee, K., Civan, F., Sigal, R., 2012. Phase behavior of gas condensates in shale due to pore proximity effects: implications for transport, reserves and well productivity. In: SPE Annu. Tech. Conf. Exhib. Texas, USA, San Antonio.

Dong, X., Liu, H., Hou, J., Wu, K., Chen, Z., 2016. Phase equilibria of confined fluids in nanopores of tight and shale rocks considering the effect of capillary pressure and adsorption film. Ind. Eng. Chem. Res. 55, 798–811.

Firoozabadi, A., 2016. Thermodynamics and Applications in Hydrocarbon Energy Production. McGraw Hill, New York.

Haghshenas, B., Soroush, M., Brohi, I., Clarkson, C.R., 2014. Simulation of liquid-rich shale gas reservoirs with heavy hydrocarbon fraction desorption. In: SPE Unconv. Resour. Conf. Woodlands, Texas, USA.

Jarvie, D., 2004. Evaluation of Hydrocarbon Generation and Storage in Barnett Shale, Fort Worth Basin. Texas. The University of Texas at Austin, Bureau of Economic logy/PTTC.

Jin, Z., Firoozabadi, A., 2016. Thermodynamic modeling of phase behavior in shale media. SPE J. 21, 190–207.

Li, Z., Jin, Z., Firoozabadi, A., 2014. Phase behavior and adsorption of pure substances and mixtures and characterization in nanopore structures by density functional theory. SPE J. 19, 1096–1109.

Linstrom, P.J., Mallard, W.G., NIST Chemistry WebBook, NIST Standard Reference Database Number 69, National Institute of Standards and technology, Gaithersburg, MD, 20899, http://webbook.nist.gov.

Lu, X., Li, F., Watson, A.T., 1995. Adsorption measurements in Devonian shale. Fuel 74, 599–603.

Luo, S., Lutkenhaus, J.L., Nasrabadi, H., 2016. Confinement-induced supercriticality and phase equilibria of hydrocarbons in nanopores. Langmuir 32, 11506–11513.

Morishige, K., Fujii, H., Uga, M., Kinukawa, D., 1997. Capillary critical point of argon, nitrogen, oxygen, ethylene, and carbon dioxide in MCM-41. Langmuir 13, 3494–3498.

Myers, J.A., Sandler, S.I., 2002. An equation of state for electrolyte solutions covering wide ranges of temperature, pressure, and composition. Ind. Eng. Chem. Res. 41, 3282–3297.

Nagarajan, N.R., Hanapour, M.M., Arasteh, F., 2013. Critical role of rock and fluid impact on reservoir performance on unconventional shale reservoirs. In: Unconv. Resour. Tech. Conf. Denver, Colorado, USA.

Nojabaei, B., Johns, R.T., Chu, L., 2013. Effect of capillary pressure on phase behavior in tight rocks and shales. SPE Res. Eval. Eng. 16, 289–281.

Nuttall, B.C., Eble, C.F., Drahovzal, J.A., Bustin, M., 2005. Analysis of Devonian Black Shales in Kentucky for Potential Carbon Dioxide Sequestration and Enhanced Natural Gas Production. University of Kentucky.

Peng, D.Y., Robinson, D.B., 1976. A new two-constant equation of state. Ind. Eng. Chem. Fundam. 15, 59–64.

Robinson, D.B., Peng, D.Y., 1978. The Characterization of the Heptanes and Heavier Fractions for the GPA Peng-Robinson Programs, Gas Processors Association. Research Report RR-28. (Booklet only sold by the Gas Processors Association, GPA).

Teklu, T.W., Alharthy, N., Kazemi, H., Yin, X., Graves, R.M., Alsumaiti, A.M., 2014. Phase behavior and minimum miscibility pressure in nanopores. SPE Res. Eval. Eng 17, 396–403.

Travalloni, L., Castier, M., Tavares, F.W., 2014. Phase equilibrium of fluids confined in pores media from an extended Peng-Robinson equation of state. Fluid Phase Equilibr 362, 335–341.

Wang, L., Parsa, E., Gao, Y.F., Ok, J.T., Neeves, K., Yin, X.L., Ozkan, E., 2014. Experimental study and modeling of the effect of nanoconfinement on hydrocarbon phase behavior in unconventional reservoirs. In: SPE Western North American and Rocky and Rocky Mountain Joint Regional Meeting, Denver, Colorado, USA.

Wang, Y., Tsotsis, T.T., Jessen, K., 2015. Competitive sorption of methane/ethane mixtures on shale: measurements and modeling. Ind. Eng. Chem. Res. 54, 12178–12195.

Wang, L., Yin, X.L., Neeves, K.B., Ozkan, E., 2016. Effect of pore-size distribution on phase transition of hydrocarbon mixtures in nanoporous media. SPE J. 19, 1096–1109.

Xiong, F., Wang, X., Amooie, N., et al., 2017. The shale gas sorption capacity of transitional shales in the Ordos Basin, NW China. Fuel 208, 236–246.

Yan, X., Wang, T.B., Gao, C.F., Lan, X.Z., 2013. Mesoscopic phase behavior of tridecane-tetradecane mixtures confined in porous materials: effects of pore size and pore geometry. J. Phys. Chem. C 117, 17245–17255.

Zhang, T., Ellis, G.S., Ruppel, S.C., Milliken, K., Yang, R., 2012. Effect of organic-matter type and thermal maturity on methane adsorption in shale-gas systems. J. Org. Geochem 47, 120–131.